



Impact of atmospheric conditions in surface–air exchange of energy in a topographically complex terrain over Umiām

Nilamoni Barman^{1,2} · Arup Borgohain¹ · S. S. Kundu¹ · Biswajit Saha² · Rakesh Roy³ · Raman Solanki⁴ · N. V. P. Kiran Kumar⁵ · P. L. N Raju¹

Received: 8 April 2018 / Accepted: 26 March 2019 / Published online: 2 April 2019
© Springer-Verlag GmbH Austria, part of Springer Nature 2019

Abstract

The effectiveness of the flux estimation techniques has been investigated over Umiām (25°40′32″N, 91°54′06″E, and altitude 1040 m above mean sea level), Shillong, in the Khasi hills located in north-east India. Primary dataset consists of sonic anemometer data recorded during January–February 2014 at 18 m and 30 m levels. Often, general planar fit (GPF) technique is used for long-term flux measurements using eddy covariance (EC). The three flux computation methods, namely double rotation (DR), GPF, and sector-wise planar fit (SPF) techniques have been compared in this investigation. SPF showed a reduction in the vertical wind (w) offset (b_0 , combination of instrument error and planar fit error) value compared to GPF. SPF minimized the planar-fit error in b_0 , while the instrument error was constant. The reduction of planar fit error has been seen in the computed sensible heat flux and momentum flux. Variations of 12–13% and 16–18% have been observed in the sensible heat flux and momentum flux in SPF compared to GPF. The effectiveness of SPF has been significant in the w -component estimation. An angle of attack (AA) which acts as a pivotal variable in the estimation of surface flux concentration varied between $\pm 6^\circ$ in all atmospheric conditions. The standard deviations of horizontal and vertical velocity normalized by friction velocity (σ_u/u^* and σ_w/u^*) as functions of atmospheric stability parameter (z/L) and obeyed a power-law relation during stable and unstable conditions. The variation in coefficients was in agreement with those estimated over flat and mountainous sites in the literature.

Responsible Editor: J.-F. Miao.

Electronic supplementary material The online version of this article (<https://doi.org/10.1007/s00703-019-00668-7>) contains supplementary material, which is available to authorized users.

✉ Nilamoni Barman
neelspinor@gmail.com

- ¹ Space and Atmospheric Science Division, Northeastern Space Applications Centre, Meghalaya 793103, India
- ² Department of Physics, National Institute of Technology, Agartala, Tripura 799046, India
- ³ Maharaja Bir Bikram University, Agartala, Tripura 799004, India
- ⁴ National Astronomical Research Institute of Thailand (NARIT), Chiang Mai, Thailand
- ⁵ Space Physics Laboratory, Vikram Sarabhai Space Centre, Trivandrum 695022, India

1 Introduction

Micrometeorological studies are essential for understanding of surface–air exchange of pollutants (Fuentes et al. 1992; Guenther et al. 1996), trace gases (Lindberg et al. 1998), ecosystem processes (Verma et al. 1986; Hollinger et al. 1994; Baldocchi and Harley 1995), carbon dioxide uptake by Earth ecosystems (Grace et al. 1995; Goulden et al. 1996; Black et al. 1996), and in energy balance. Excessive run-to-run changes in scalar fluxes and energy balance are a serious concern of surface flux observations and are a genuine issue of complex terrain (Lee 1998). In a spatial domain, the net surface flux consists of turbulent and mesoscale parts (Avisar and Chen 1993; Mahrt and Sun 1995; Lee 1998). The heterogeneity in the surface cover (e.g., irregular vegetation and artificial structures) and the topography account for the remarkable influence on the circulation of the wind and measurements of turbulent fluxes, e.g., sensible heat flux (H , conductive heat flux from the earth's surface to the atmosphere) and momentum flux (τ , rate of change of horizontal momentum which is moving

across a unit area) (Moraes et al. 2005; Vickers and Mahrt 2006; Rotach and Zardi 2007; Bianco et al. 2011; Solanki et al. 2016).

Using the eddy-covariance (EC) method, surface turbulent fluxes can be directly measured using fast response sensors like sonic anemometers. Over the complex terrains, extreme care has to be taken when calculating the fluxes using the EC method. Normally, the wind vectors are measured by sonic anemometer probes in a reference frame vertical with gravity. The sonic anemometer cannot be leveled perfectly, such that its upright w -axis is constantly perpendicular to the mean flow. It is essential to choose a suitable frame of reference for the accurate measurements of vertical wind components (w) and hence the flux measurements, to minimize the cross-contamination between velocity components (Lee et al. 2004). This becomes more important when the sensor is placed in a sloping terrain where the magnitudes of the streamwise fluctuations not only affect the mean velocity but also contribute significantly to the errors in the estimation of fluxes (Wilczak et al. 2001). It is, therefore, essential that before analyzing the fluxes for a meaningful interpretation, the measurements are to be transformed into an appropriate terrain-following coordinate system (Yuan et al. 2011).

There are different methods that are used to achieve this, namely double rotation (DR) or triple rotation (TR) to the planar fit (PF) coordinate system (McMillen 1988; Wilczak et al. 2001). DR has issues in the computation of surface fluxes, i.e., over-rotation, information loss, retrogression of data quality (Wilczak et al. 2001; Lee et al. 2004; Foken et al. 2004; Rebmann et al. 2012). TR is effective only at an ideal site with zero advection. For a non-ideal location having several wind flows (McMillan 1988; Yuan et al. 2007), one cannot anticipate the same direction between mean flow and stress over a mountainous site, i.e., one cannot assume $v'w'=0$ which is used in TR. Specifically, at a non-ideal station, the over-rotation decreases the quality of the dataset and provides an inappropriate estimation of surface fluxes (Finnigan et al. 2003; Lee et al. 2004; Yuan et al. 2007). Over the mountainous sites, due to the thermal circulation and free convection, 1-D wind flow behaves as 2-D and 3-D flows and can generate a non-zero mean w -component (Lee 1998; Finnigan 1999). Berger et al. (2001) demonstrated that within 30 m of height from the Earth's surface, flux measurements do not vary considerably within a period of 30 min, so a half-hourly flux averaging period is sufficient for all flux scales within that height. In such case, over-rotation provokes a systematic error in the flux estimation (Yuan et al. 2011). In addition, the random sampling error of surface fluxes is comparably higher in the DR under low wind conditions (Wilczak et al. 2001; Stiperski and Rotach 2016). Mostly, H is less susceptible to tilt error than τ (Lee et al. 2004). Stiperski and Rotach (2016) reported that H

during day hours (positive H) is sensitive to tilt correction. Heat flux, however, is led by buoyancy that moves along the geopotential, i.e., the work that must be performed against the Earth's gravitational field to lift 1 kg of an air mass from sea level to that point. Within ABL at a certain height, the dominant H is 'upward' rather than perpendicular to the local slope. Turnipseed et al. (2003) carried out a detailed comparison of DR, TR, and PF methods at a forest site over a hilly terrain and reported that no significant variation observed among the fluxes. Yuan et al. (2011) and Kral et al. (2014), also reported no significant differences in DR- and PF-computed sensible heat flux.

The general planar fit (GPF) or PF method is a right-hand orthogonal coordinate system and utilizes a collection of each half-hourly measurements of wind components (u , v , and w). Based on the measured mean wind components during the observational period, a fitted plane is found by applying multiple linear regression. GPF rotation can establish a stable coordinate frame and reduces the over-rotation due to the flow distortion by instruments and tower structure to furnish information on the 2-D and 3-D flows. The GPF technique applies for coordinate rotation on the eddy-covariance flux calculation (Lee et al. 2004) and shows a better result over local topography that follows a surface with small curvature than the other techniques.

GPF also has drawbacks; large numbers of the data points in a distinct direction play a vital role in the flux computation (Finnigan et al. 2003). The planar fit coordinate system is usually affected by the complexity of the terrain (varying wind directions); so GPF tilt correction will be influenced by the prevailing wind sectors. (Yuan et al. 2007; Shimizu 2015; Oldroyd et al. 2016). The wind flow is influenced by the wind direction in such complex terrain and so the issues can be partially resolved by the sector-wise planar fit (SPF) (Finnigan et al. 2003; Ono et al. 2008; Paw et al. 2000; Siebicke et al. 2012; Li et al. 2013; Shimizu 2015). Over a complex topography, as SPF is executed for discrete wind sectors, the wind-direction-dependency on the tilt corrections is reduced (Ono et al. 2008; Paw et al. 2000; Shimizu 2015; Li et al. 2013; Oldroyd et al. 2016). So, the SPF technique can minimize the terrain-induced signal from the time-series data and can diminish the tilt correction between velocity components (Oldroyd et al. 2016). For tilt correction, SPF requires enough dataset to compute a reliable planar fit coefficient in each sector.

The prime motivation behind this work was the utilization of an appropriate existing technique for eddy-covariance method and observation of surface air exchange of energy in different atmospheric conditions at a remote mountainous location in the north-east India. The Present study is a part of the "Network of Observatories for Boundary-Layer Experiments" (NOBLE) project of Indian Space Research Organization (ISRO) Geosphere-Biosphere Program (GBP)

program to understand the boundary layer dynamics over different geographical regions of India. The present study is the first of its kind over this complex terrain in the north-east India.

2 Observational site, instrumentation, and methodology

2.1 Experimental site and prevailing meteorology

The experiment was carried out using a 31-m meteorological tower-based instrumentation. The experimental setup is within the premises of North Eastern Space Applications Centre (NESAC) at Umiam, Shillong (25°40′0.32″N, 91°54′0.06″E, and altitude 1040 m above mean sea level) in the Khasi hills located in north-east India. The slope of the hill extends along the north–south direction. The peak of the Khasi hills has an altitude of about 1950 m and is located ~20 km south-east of the station. The slope within a horizontal distance of 1 km is about 5°–6° towards the east and south-east direction of the hill peak (where the tower is located). The slope and valley are largely covered with pine trees. The slope towards the north is limited within 1 km horizontal distance, whereas a 2° slope exists towards the south-west, primarily for the upwind during winter season. The average height of the trees is about 5.5 meters in south-east and south-west directions. Small grass and bushes also exist in the areas adjacent to the tower. January is the coldest month when the minimum temperature falls to 3 °C with mean air temperature of 14.5 °C. The relative humidity varies from 45 to 89% with moderate winds (1.5–4.0 m s⁻¹) blowing from the western and eastern zones throughout the season (Fig. 1).

2.2 Instrumentation and methodology

CSAT3 sonic anemometers were installed at four levels (6, 10, 18, and 30 m above ground level) on a 31-m meteorological tower for flux measurements. Only the data from 18 and 30 m levels have been used for analysis. Data could not be collected at 10 m due to a technical problem. The 6-m level is undoubtedly within the roughness sublayer and may be affected by nearby roughness elements. Data from 1st January to 28th February 2014 (total 43 cloud-free days) at both the levels were used for analysis after comprehensive quality checking. In this study, 2064 numbers of 30-min mean data sample of wind components have been used. Out of 2064 samples, 1399 and 563 numbers belong to the sector of 30°–175° and 220°–330°.

The CSAT3 sensors have been calibrated in the laboratory before installation on the 31-meter meteorological tower. Wind components (u , v and w) and acoustic temperature (T) are

computed utilizing the probes operating at 25 Hz. The CSAT3 is embedded with a 3-D head-correction for an angle of attack (AA) between $\pm 60^\circ$. AA is the angle between the wind vector and the instrument horizontal (McBean 1974; Wilczak et al. 2001; van der Molen et al. 2004; Yuan et al. 2007). The correction terms embodied in the sensors are estimated by conducting the wind-tunnel tests and implemented by the manufacturer. This function corrects the flow distortion of the sensor head based on u and w wind components. The errors induced by wind flow normal to the sonic direction are rectified instantly before the wind speed is converted into orthogonal wind components and not required to employ the sound speed correction (CSAT3 2014). The sonic virtual temperature (T_v) is computed by the sensors with the following relationship: $T_v = \frac{c^2}{\gamma_d R_d} - 273.15$, (where c is the speed of sound in air, γ_d is the ratio of specific heat of dry air at constant pressure and volume and gas constant in dry air is $R_d = 287.04 \text{ J K}^{-1} \text{ kg}^{-1}$). T is calculated using the equation $T \approx T_v - 0.02 p$ (where p is the partial pressure due to moisture). For estimation of p , the relative humidity measurements are acquired from the humidity sensor.

2.3 Coordinate rotation method

This section describes a general methodology for estimation of coefficients, pitch, and roll angle which are primarily required for the transformation of coordinate systems using various methods (DR, GPF, and SPF).

The measurements over complex terrain have to be properly corrected for sensor tilt for meaningful interpretation by choosing proper coordinate systems. The wind flow in the complex terrain has to be converted to streamline-following coordinate systems as they follow the terrain following coordinate systems (Wilczak et al. 2001). The eddy covariance (EC) method for flux calculation is primarily used for the true horizontal and vertical winds over homogenous terrains corrected by DR and TR, whereas, for complex terrain, local terrain for EC is not usually leveled and requires proper transformation to streamline flow.

Over complex terrain, the measurements of vertical velocity components are influenced by the local terrain slope and sensor tilt, and local circulation (Lee 1998). Using multiple linear regressions (MLR) analysis, the coordinate rotation can establish a proper coordinate framework and overcome the contamination of mean wind flow (Wilczak et al. 2001; Yuan et al. 2007; Mammarella et al. 2007)

Coordinate rotation technique can be initiated with MLR using the following equation:

$$w_r = b_0 + b_1 u_r + b_2 v_r, \quad (1)$$

where u_r , v_r , and w_r are the 30 min averaged raw data of orthogonal wind components recorded by the sonic

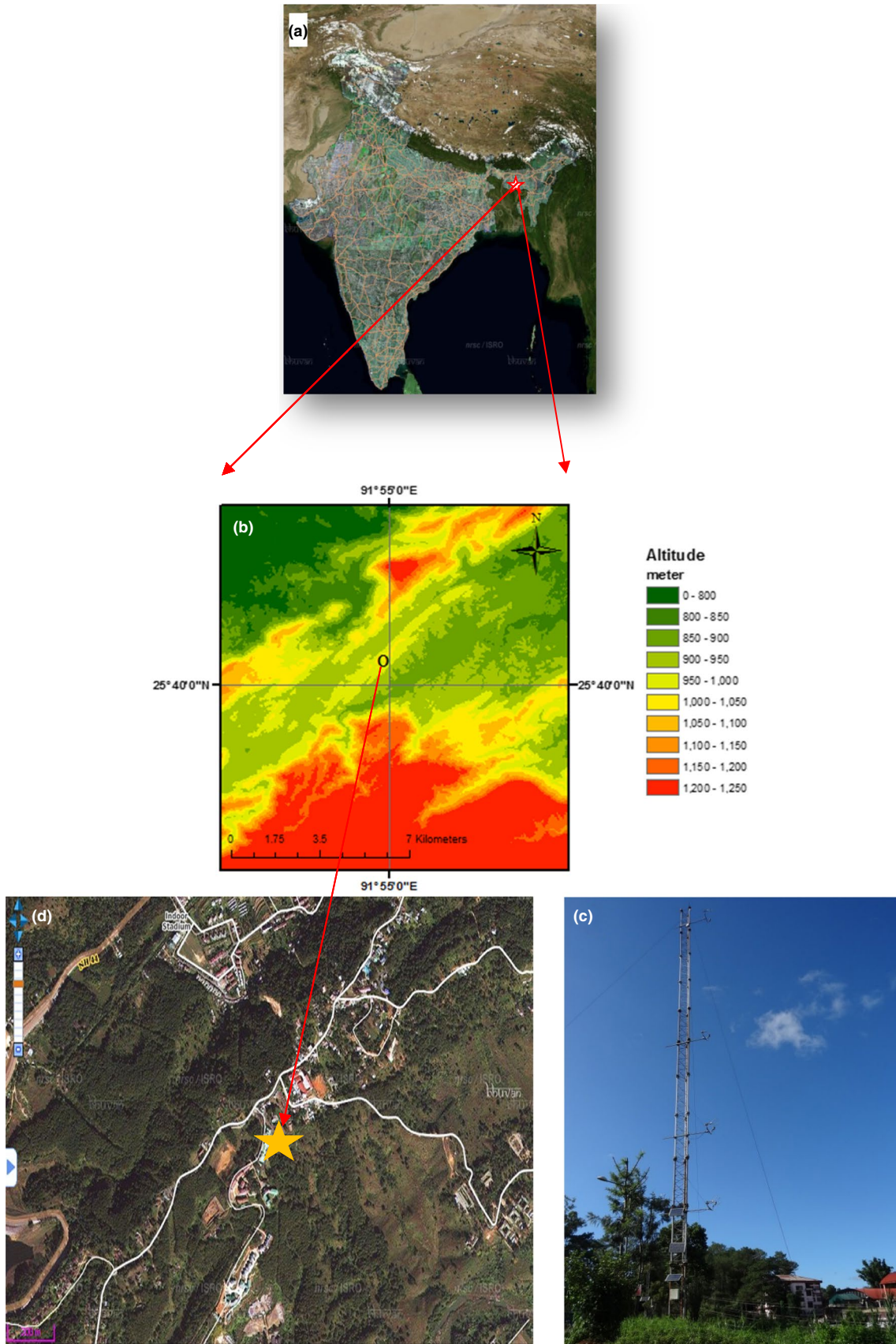


Fig. 1 **a** Location of NESAC (marked by a red star) on the map of India, captured from Bhuvan portal (NRSC, ISRO), **b** represents topographical map of the location (marked with a black circle) captured from Bhuvan portal (NRSC, ISRO) CARTOSAT-1 digital elevation model (DEM), **c** photograph of the tower with reference to ground captured at a distance of 50–60 m away from the tower at the north-east direction, and **d** satellite image of the measurement site

anemometer and b_0, b_1, b_2 are the regression coefficients computed from the MLR (Wilczak et al. 2001; Yuan et al. 2007; Mammarella et al. 2007). b_0 is a w -offset value, probably due to the instrument error and error by fitting a single plane to the dataset. b_1 and b_2 are the weighted contribution of zonal (u) and meridional (v) wind towards w (Wilczak et al. 2001; Yuan et al. 2007). In complex terrain, different slopes exist in different directions and the wind flow is influenced by these slopes. So, we have to use slope correction to the wind component to make the wind flow parallel for the sensor and these slope corrections are represented by the pitch angle (α) and roll angle (β) for the site (Yuan et al. 2011). α and β are the fixed angles required to rotate the sonic anemometer into a plane parallel to that of the local terrain slope. α and β are computed from b_1 and b_2 as follows:

$$\alpha = \sin^{-1} \left(\frac{b_1}{\sqrt{b_1^2 + b_2^2 + 1}} \right), \tag{2}$$

$$\beta = \tan^{-1} (b_2). \tag{3}$$

Subsequently, these values have been utilized for the tilt corrections and calculations of surface fluxes at the station. The following equations have been used for the tilt correction of orthogonal wind components:

$$u_c = u_r \cos \alpha + v_r \sin \alpha \cdot \sin \beta - \sin \alpha \cdot \cos \beta (w_r - b_0), \tag{4}$$

$$v_c = v_r \cos \beta + \sin \beta (w_r - b_0), \tag{5}$$

$$w_c = u_r \sin \alpha - v_r \cos \alpha \cdot \sin \beta + \cos \alpha \cdot \cos \beta (w_r - b_0), \tag{6}$$

where $u_c, v_c,$ and w_c are the corrected $u, v,$ and w wind components. The corrected wind components are used for flux computations. The quantities $H, \tau,$ friction velocity (u_*) and atmospheric stability parameter (z/L) are computed as follows:

$$H = \rho C_p \overline{(w'_c \theta'_v)}, \tag{7}$$

$$\tau = \rho \sqrt{\overline{(u'_c w'_c)^2} + \overline{(v'_c w'_c)^2}}, \tag{8}$$

$$u_* = \sqrt{\frac{\tau}{\rho}}, \tag{9}$$

$$\frac{z}{L} = z / \left(\frac{-u_*^3}{k \frac{g}{\theta_v} w'_c \theta'_v} \right), \tag{10}$$

where $\rho, C_p, u'_c, v'_c,$ and w'_c are atmospheric density, the isobaric specific heat of air, and fluctuation of the corrected orthogonal wind components. In $z/L, L = \left(\frac{-u_*^3}{k \frac{g}{\theta_v} w'_c \theta'_v} \right),$ where $\theta_v, \theta'_v, k,$ and g are virtual potential temperature, fluctuation of virtual potential temperature, Karman constant (0.4), and gravitational acceleration. z is the observational height and L is the Obukhov length (Monin and Obukhov 1954). Obukhov length is the elevation above the ground where the turbulence developed by thermal motions exceeds the turbulence generated by the wind shear (Stull 1988).

2.4 Data quality check

The quality checking of half-hourly flux data was performed using two standard tests that are primarily used in complex terrain, i.e., the stationary test (ST) and integral turbulence characteristics test (ITC) (Foken and Wichura 1996). The stationarity implies that the statistics do not vary with time and absence of stationarity is one of the major problems in the turbulence measurements (Foken and Wichura 1996). In this exercise, to investigate the turbulence statistics under the platform of Monin–Obukhov similarity theory, we have considered only those fluxes that are measured under the condition of mean wind speed (U) > 1 m s⁻¹. Here, we have highlighted ITC to represent the turbulence characteristics over the station, not for data quality aspects. The occurrence of non-stationary motions shows a high dependency on U rather than stability and decreases as U increases (Liang et al. 2014).

The ST test compares the mean flux values over each half-hourly interval with the mean values over the six corresponding 5-min sub-intervals. In the present study, based on ST test, 70% and 85% input dataset passed the quality checks dataset at 18 m and 30 m heights, which are considered for the further analysis.

In this paper, we tested three different methods, namely DR, GPF, and SPF over this location by considering the wind flow from different directions (dominant wind flow for SPF and wind flow from all directions for GPF method) and compared the methods. First, we present the dominant wind pattern which prevails over this region in the next section.

3 Results and discussion

3.1 Wind variability at the experiment site

Figures 2 and 3 describe the wind rose diagram and the frequency distribution of wind speed, respectively. Prevailing winds are mostly seen in the three dominant wind sectors of 30° – 90° , 90° – 175° , and 220° – 330° (Fig. 2). Figure 4 reveals that the wind flow at the station is governed primarily by a mountain-valley wind circulation. We have considered the sector of 30° – 90° and 90° – 175° as one because the slopes in that direction were in the range of 5° – 6° . The influence of the slope on the wind, therefore, would be the same. Another reason could be that SPF needs higher number of data points for reliable results for the particular wind sector. A detailed study was taken up using the corrected dataset to improve the quality of analysis. From Fig. 4, it is observed that the

dominant nighttime south-easterly winds gradually changed to southerly after an hour of sunrise. As day progress, wind speed increased gradually and a noticeable shift could be observed towards the south-west which remained till local noon (1130 IST, India standard time = UTC + 5:30 h). Thereafter, the wind gradually changed to south-easterlies and remained more or less south-easterlies throughout the night till sunrise except for one and a half hours from 0000 to 0130 IST, where it changed to north-easterlies. Interestingly, high horizontal wind speed was observed during nighttime (0000–0600 IST). Wind speed gradually increased during daytime and reached its maximum value around 0800 IST and gradually decreased thereafter till it reached diurnal minimum around 1600 IST. Thereafter, horizontal wind speed increased and remained moderate throughout the nocturnal period. It is interesting to see an increase in horizontal wind speed around 1400 IST.

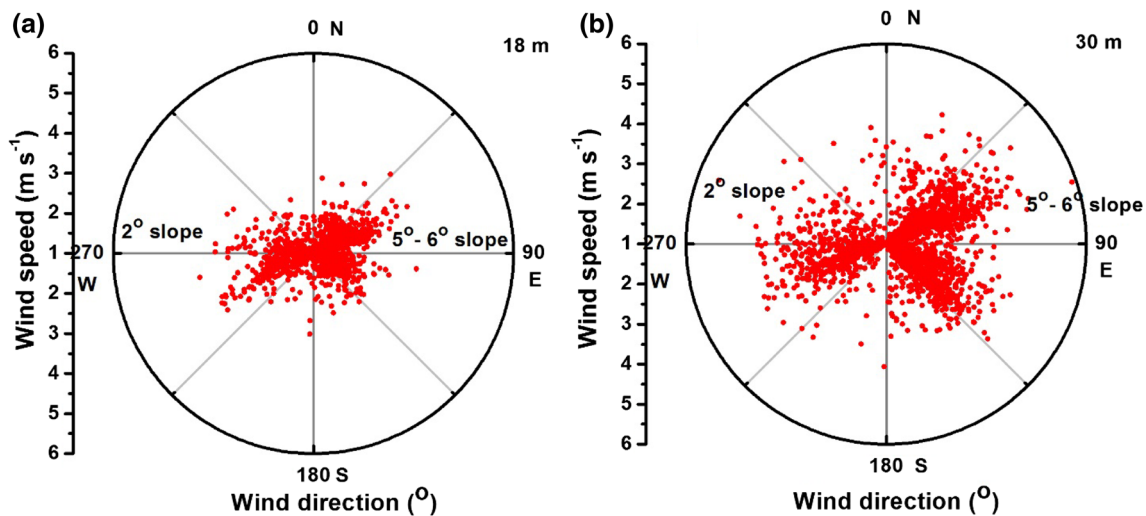


Fig. 2 Wind rose plots for the observational period at the 18 m (a) and 30 m (b) heights

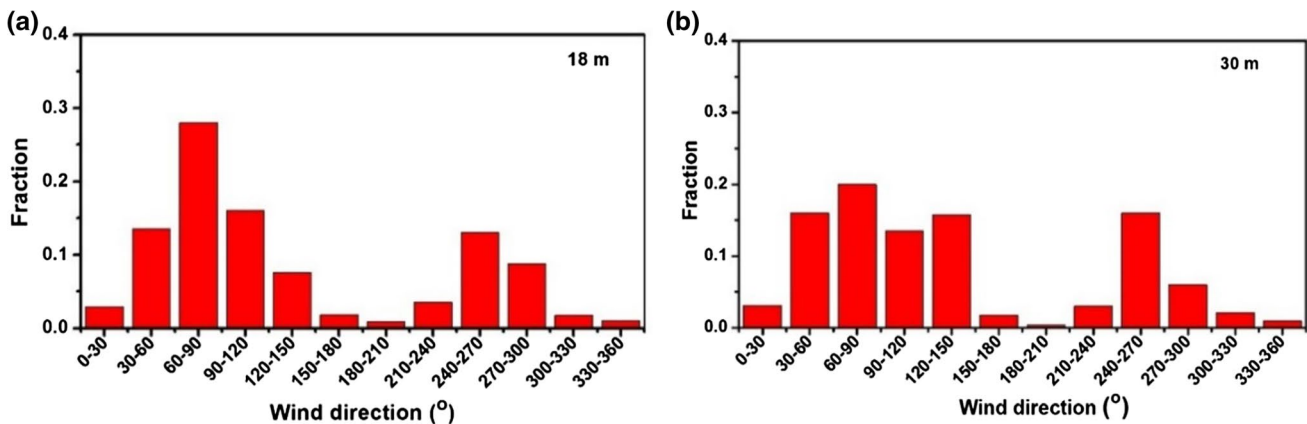


Fig. 3 Frequency distribution of wind at the 18 m (a) and 30 m (b) heights

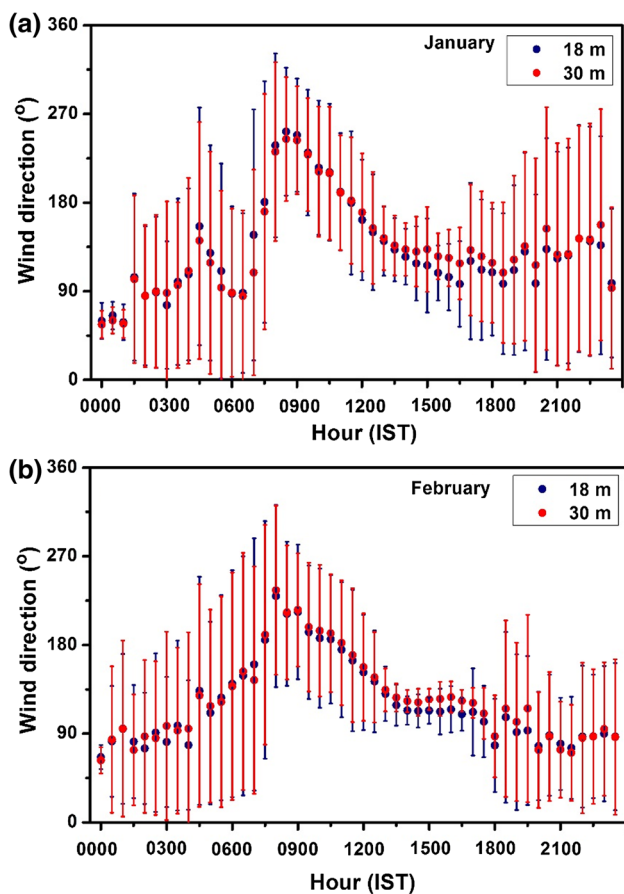


Fig. 4 The diurnal variation of monthly mean (solid circle) and standard deviation (bar) of wind direction in January (a) and February (b) at the 18 m (in navy blue) and 30 m (in red) heights

From Figs. 4 and 5, it can be concluded that during the hours between 1400 and 0600 IST, prevailing wind flowed from the sector of 30° – 175° , whereas during the day hours between 0630 and 1330, IST wind flowed from the sector of 220° – 330° . The shifting of prevailing wind flowed from the sector of 30° – 175° to 220° – 330° in different time periods that indicated a mountain valley wind circulation at the station (Fig. 4). The wind speed reached the lowest magnitude when wind direction shifted from 30° – 175° to 220° – 330° during 0730–0830 IST, and from 220° – 330° to 30° – 175° during 1700–1800 IST, at both heights in January and February, respectively.

3.2 Variability of PF coefficients

In this study, we have used two types of PF methods, i.e., GPF and SPF. In GPF, the raw wind velocity components considered for computation of PF coefficients, the value of b_0 obtained for the period being -0.037 m s^{-1} and -0.047 m s^{-1} at the 18 m and 30 m, respectively. SPF is a modified version of GPF, where the dataset were divided

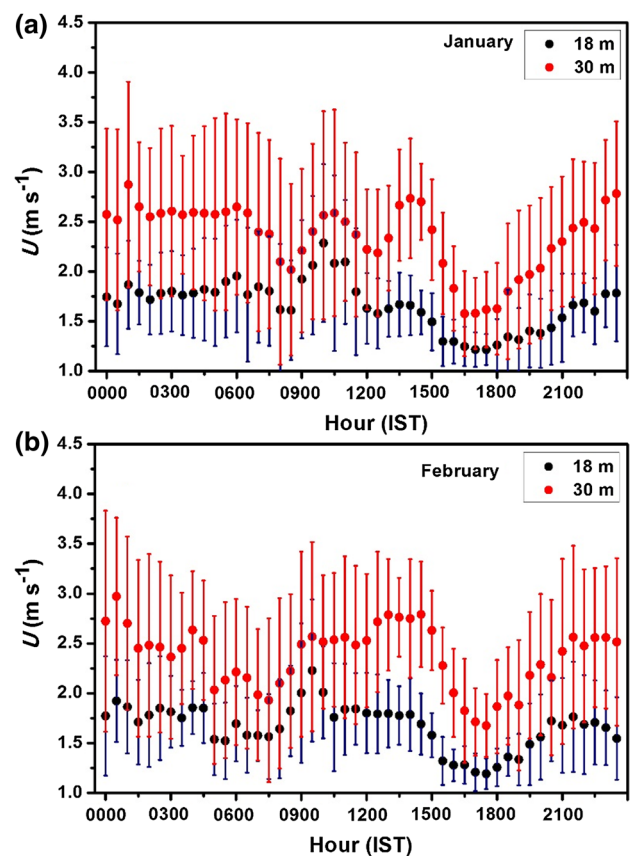


Fig. 5 The diurnal variation of monthly mean (solid circle) and standard deviation (bar) of mean wind speed (U) in January (a) and February (b) at the 18 m (in navy blue) and 30 m (in red) heights

in the different dominant wind sectors (30° – 175° and 220° – 330°) and followed by an application of PF method. For each sector, b_0 , b_1 , and b_2 were computed following PF approach of Wilczak et al. (2001). b_0 value from the SPF technique was $+0.001 \text{ m s}^{-1}$ when east and south-easterly flows (30° – 175°) were dominant and $+0.003 \text{ m s}^{-1}$ when westerly (220° – 330°) wind was flow dominant at 18 m level. Similarly, b_0 was about -0.029 m s^{-1} when wind flows from the east and south-east direction and $+0.017 \text{ m s}^{-1}$ when wind is coming from the west direction for 30 m level. b_0 computed using SPF was negligible compared to that computed using GPF. Besides the two sectors mentioned above, other sectors did not have enough data points to apply the SPF technique. For GPF the b_0 value cannot differentiate between the instrument error and the PF error. For SPF, b_0 was smaller compared to GPF primarily for the reduction in the PF error by utilizing different wind sectors. Ideally, instrument error of b_0 would be the same for each sector, signifying that the PF error was resolved exclusively. In practice, this does not happen and there will always be a mix of instrument error and some PF error. Refining sectors might help eliminate

this if there are sufficient data. Of course, all this assumes that the instrument error is constant and independent of wind direction, which may not be the case if it is induced by the structure of the sonic anemometer or by a large (wind direction dependent) angle of attack. From the results, at 18 m, b_0 values of SPF reduced tremendously compared to GPF, which indicates SPF eliminated PF error from the b_0 values, whereas at 30 m, b_0 values are smaller than GPF. The b_0 values through SPF were bigger at 30 m level than that of 18 m level, respectively. One of the reasons is that, at 30 m, the instrumental error is higher than PF error, which has not been reduced by SPF.

The differences between the coefficients of GPF and SPF are shown in Table 1.

3.3 Comparison of surface fluxes by DR, GPF, and SPF methods

Figure 6 shows a comparison of the surface fluxes calculated by the DR and PF methods (GPF, SPF). Sensible heat flux is a land surface- and topography-dependent surface-layer parameter (Stiperski and Rotach 2016). At night time, H was negative that coincided with the periods of downslope wind at the station (Fig. 6a, b). Additionally, nighttime mean H

Table 1 Coefficients comparison of SPF vs GPF technique

Planar fit method	Sector	18 m			30 m		
		α	β	B_0 (m s^{-1})	α	β	B_0 (m s^{-1})
SPF	30°–175°	−7.41°	−0.37°	0.001	−5.56°	0.62°	−0.029
	220°–330°	−2.29°	1.83°	0.003	−1.95°	0.68°	0.017
GPF	0°–360°	−4.27°	0.36°	−0.037	−4.08°	0.97°	−0.047

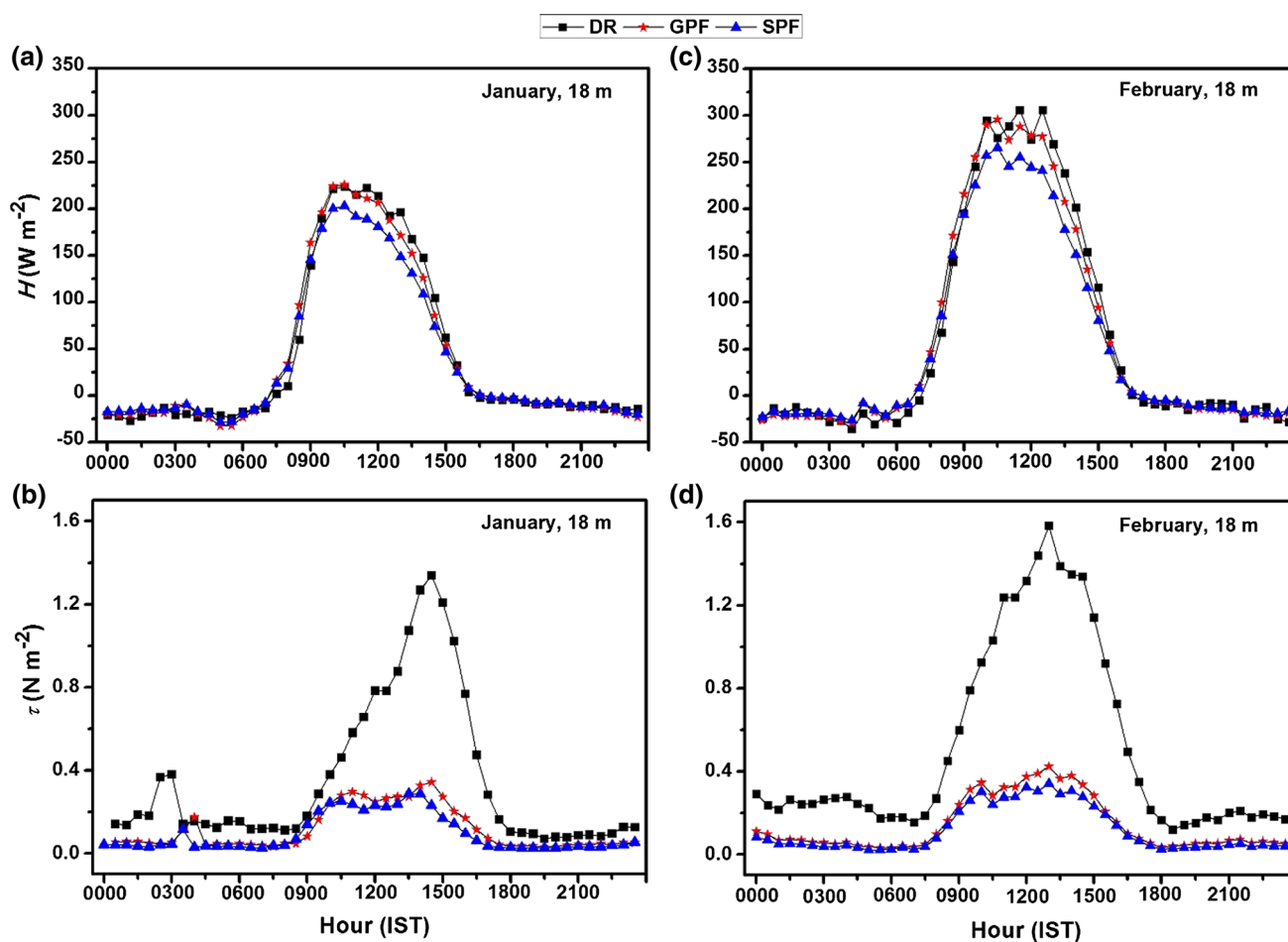


Fig. 6 Comparison of DR (in black), GPF (in red), and SPF (in blue) computed monthly mean values of H (a, c), and τ (b, d) in January and February at the 18 m height

computed with DR ($-21 \pm 24 \text{ W m}^{-2}$ and $-18 \pm 8 \text{ W m}^{-2}$) and GPF ($-21 \pm 19 \text{ W m}^{-2}$ and $-19 \pm 7 \text{ W m}^{-2}$) was larger negative than the SPF ($-18 \pm 17 \text{ W m}^{-2}$ and $-17 \pm 6 \text{ W m}^{-2}$) values in January and February at 18 m level. While during daytime, the SPF ($115 \pm 74 \text{ W m}^{-2}$ and $160 \pm 94 \text{ W m}^{-2}$) yielded smaller positive H values compared to DR ($150 \pm 73 \text{ W m}^{-2}$ and $215 \pm 83 \text{ W m}^{-2}$) and GPF ($130 \pm 82 \text{ W m}^{-2}$ and $182 \pm 106 \text{ W m}^{-2}$) values in January and February at the 18 m level. Stiperski and Rotach (2016) found larger negative H values in DR compared to GPF in the night time, whereas in daytime PF computed larger positive H fluxes than DR. They also reported a systematic discrepancy between fluxes obtained with GPF and SPF. The SPF provided identical results as DR, the same as for the H and τ in a mountainous site. In our case, SPF yielded lesser H values compared to DR and GPF. The PF error in the flux data has been removed by moving from GPF to SPF technique. There was 12.4% variation in H fluxes during daytime (0800–1600 IST), whereas 13% variation has been observed between GPF and SPF in the night time at both the levels. The difference between H computed with DR and PF techniques indicates surface heterogeneity and hence ‘local advection’ at the station and can mostly be connected to slope winds. The greater discrepancy between DR and PF techniques is most pronounced for large positive sensible heat fluxes (unstable upslope flow), when $\overline{w'_c \theta'_v}$ is small but positive. These results can be associated with hot-air advection ($\theta'_v > 0$) in the upslope flow and thermals that split from the surface.

In Fig. 6, DR shows larger values compared to PF methods for τ . DR has overestimated the τ values significantly compared to SPF, whereas GPF shows less variations in τ during day hours when the wind direction variability is higher (Fig. 6c, d). DR assigns w to the sensor tilt and works

in leveling the sonic anemometer. Hence, DR allows only 1-D conditions of a vertical gradient, because 2-D and 3-D flow, such as convective circulation, can produce nonzero w . Here, in an unstable atmospheric condition, DR overestimated the τ values compared to the stable condition. The higher τ values occurred in 1100–1400 IST and prevailing wind direction was from the sector of 100° – 150° with the moderate wind speed. During the day hours higher vertical convective motion and moderate wind at the site transform the 1-D flow to 2-D and 3-D flow. In the daytime, as the vertical convection increases, the overestimation of τ values also increases in DR computation (Fig. 7). In DR computation, 16% of τ values are higher than 1 N m^{-2} , which occurred due to the higher convective motion in the daytime. Here, over-rotation (because of instrument offset in the measurement of w) results in the systematic bias in the surface-flux computation, especially in τ values. Moreover, the random sampling error of surface fluxes is comparatively greater in the DR under low wind atmospheric conditions due to finite averaging time. The existence of surface heterogeneity and ‘local advection’ ($\overline{v'_c w'_c}$) of higher air movement cause higher difference between DR and PFs; probably, an SPF largely resolves the overestimation of the DR and GPF approach at the station with a moderate slope, which occurred because of the direction-dependent non-uniformity in the various wind sectors. From this, it can be concluded that τ is very much sensitive to the crosswind contamination at the station. The uncertainties in flux data due to GPF have been removed with assistance of SPF technique. A variation of 16% and 18% variation has been observed in τ at the 18-m and 30-m heights. The largest difference between DR and PF techniques (Fig. 6c, d) has been easily observed for moderate wind speeds (Fig. 5). Stiperski and Rotach (2016) demonstrated a greater difference in τ between DR and PF

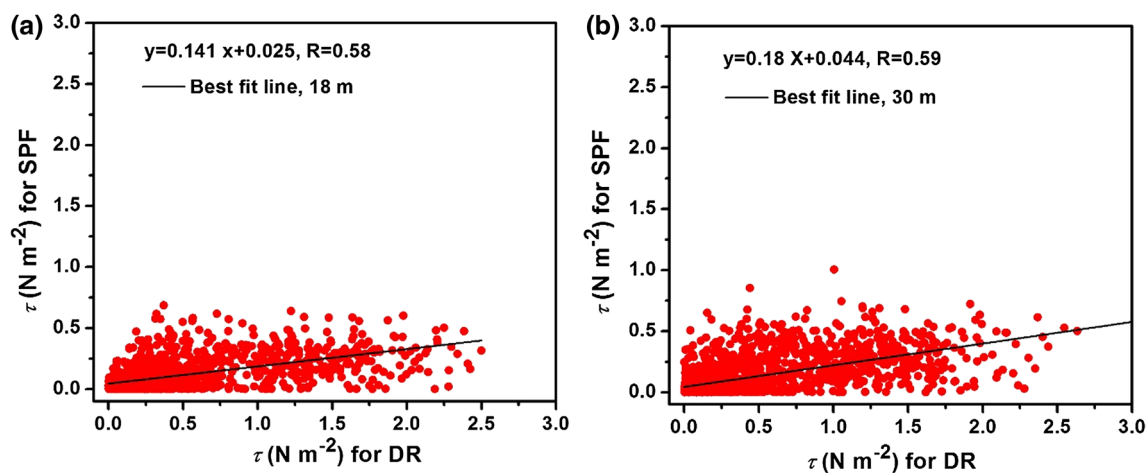


Fig. 7 The correlation between DR and SPF at the 18 m (a) and 30 m (b) level

techniques due to the higher wind speed at complex terrain. They further recommended that, apart from SPF in complex terrain, a wind-speed dependent PF is still required to eliminate the prejudices of wind-speed dependent flow separation that might occur for various slopes.

3.4 Variations of normalized standard deviations

With an aim to verify the applicability of Monin–Obukhov Similarity Theory (MOST) for the observations, we considered the standard deviations of the wind-velocity normalized with frictional velocity, i.e. (σ_u/u_* and σ_w/u_*) (Foken et al. 1991; Foken and Wichura 1996; Geissbuhler et al. 2000; Solanki et al. 2016). The variations of σ_w/u_* were considered for the data quality and integral turbulence characteristics under different stability conditions (z/L) over hilly terrains (Foken and Wichura 1996).

The diurnal variations of monthly mean z/L parameter for the observation period is presented at 18 m and 30 m levels are shown in Fig. 8. The stable ($z/L > 0$) conditions prevail during the late evening and nocturnal time, whereas

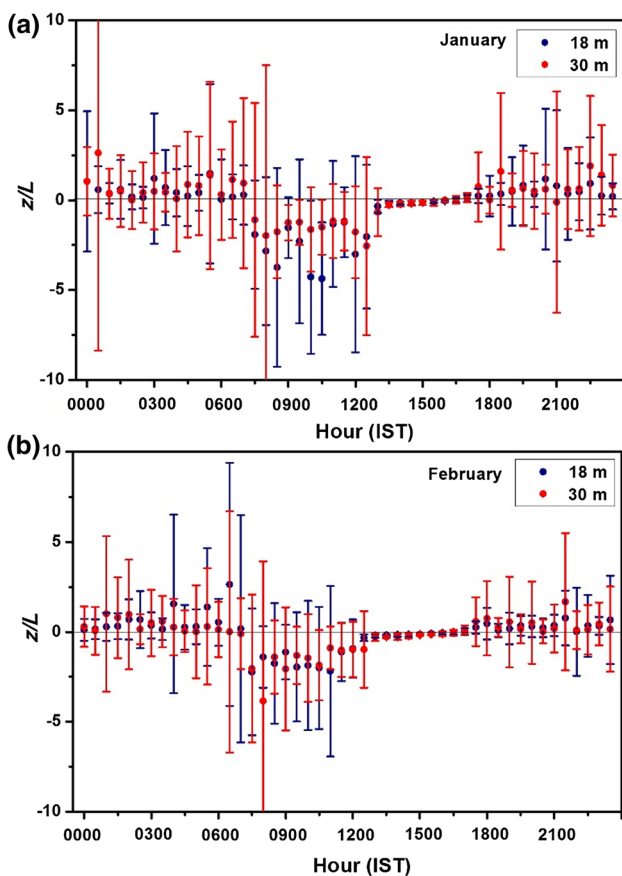


Fig. 8 The diurnal variation of monthly mean (solid circle) and standard deviation (bar) of z/L in January (a) and February (b) at the 18 m (in navy blue) and 30 m (in red) heights

unstable condition ($z/L < 0$) prevails during the daytime. Interestingly, the atmospheric conditions during local noon changed to neutral ($z/L \approx 0$) which prevailed until evening hours. We attribute these noontime variations in the atmospheric stability to the gradual shift in the direction of winds associated with the mountain valley circulation (this aspect was investigated using a balloon-borne campaign over this location and will be addressed in later article). From Figs. 4 and 8 it is evident that, during unstable (neutral to stable) conditions, dominant winds flow in the sector 220° – 330° (30° – 175°) over this site. Under these dominant wind sectors and stability conditions, quality of the data and integral turbulence characteristics were investigated for the different angles of attack (AA) ($\pm 10^\circ$) at the 18 m height level that are being presented in the following sections.

3.4.1 Integral turbulence characteristics

Figure 9 shows the variations of bin-averaged σ_u/u_* and σ_w/u_* with z/L for stable ($z/L > 0$) and unstable ($z/L < 0$) conditions for -10° AA $< 10^\circ$ at the 18 m level. Results for different AA are shown to examine any inconsistency in the observations as a function of AA. The red solid curve represents the variations derived by Foken and Wichura (1996). The blue solid curve has been shown the best curve fit using the relation given by (Foken et al. 1991; Foken and Wichura 1996):

$$\frac{\sigma_i}{u_*} = A \left(\left| \frac{z}{L} \right| \right)^B, \quad (11)$$

where A and B are fitted parameters and $i = u$ and w . The fitted values obtained for the present study are given in Table 2. It is observed that the variations of both σ_u/u_* and σ_w/u_* with z/L show consistency and are mostly within the $\pm 10\%$ of Foken and Wichura (1996) and can be considered of good quality.

3.5 Flux angle distribution

The flux-angle distribution is defined as the variation of flux with the angle of attacks (AA). Flux angle distribution can be used to infer the process of flux transport like an increase (decrease) in the scalar flux concentration or momentum by correlating with the upslope (downslope) (McBean 1974; Motha et al. 1980; Gash and Dolman 2003).

Figure 10 shows the diurnal variation of mean AA to mean H and τ for the observational period at 18 m level. Results show that the variations of mean AA are different under different stability conditions. Table 3 provides the mean and standard deviation of AA, H , and τ under unstable, neutral, and stable conditions. During all atmospheric conditions (unstable, stable, and neutral) conditions AA varied between $\pm 6^\circ$. It is

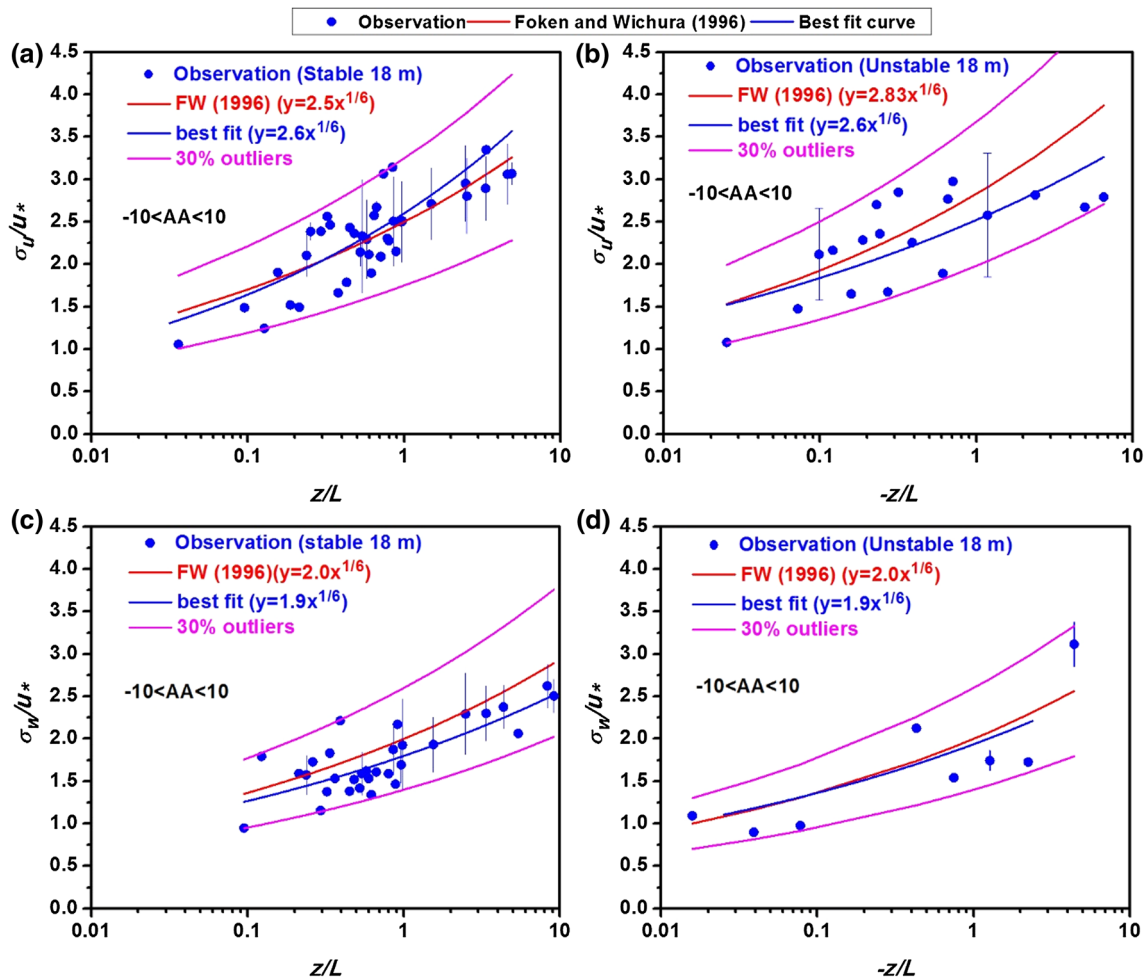


Fig. 9 Normalized standard deviation of u (a, b) and w (c, d) under stable and unstable conditions for $-10^\circ < AA < 10^\circ$ at the 18 m height

Table 2 Comparison of empirical model and observed values at the station

Relationship	Stable condition		Unstable condition	
	u	w	u	w
Foken and Wichura (1996) and Foken et al. (1991)	$2.5 \left \frac{z}{L} \right ^{1/6}$	$2 \left \frac{z}{L} \right ^{1/6}$	$2.83 \left \frac{z}{L} \right ^{1/6}$	$2 \left \frac{z}{L} \right ^{1/6}$
Observation at 18 m ($-10^\circ < AA < 10^\circ$)	$2.6 \left \frac{z}{L} \right ^{1/6}$	$1.9 \left \frac{z}{L} \right ^{1/6}$	$2.6 \left \frac{z}{L} \right ^{1/6}$	$2 \left \frac{z}{L} \right ^{1/6}$
Observation at 30 m ($-10^\circ < AA < 10^\circ$)	$2.5 \left \frac{z}{L} \right ^{1/6}$	$1.8 \left \frac{z}{L} \right ^{1/6}$	$2.4 \left \frac{z}{L} \right ^{1/6}$	$1.7 \left \frac{z}{L} \right ^{1/6}$

found that during positive (negative) AA there was an increase (decrease) in both flux concentration and H . Present results highlight that positive (negative) AA were associated with the upslope (downslope) over the complex terrain and were in tune with observations from complex terrain (McBean 1974; Gash and Dolman 2003).

4 Conclusions

In the present work, an attempt has been made to understand the implication of SPF technique to the flux dataset. Over complex terrain, practically it is essential to segregate the dataset as per prevailing wind directions for correction of the flux data. SPF technique expands the assumption of the PF technique to include the impacts of

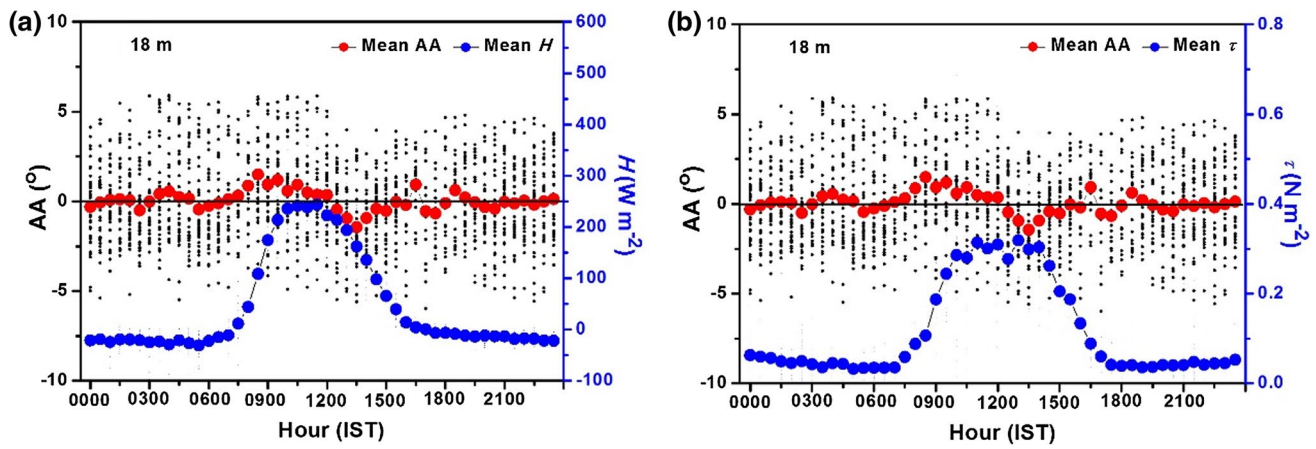


Fig. 10 Dependency of H (a) and τ (b) concentration on mean AA (red circle) for the observational period at the 18 m heights

Table 3 Values of AA, H , and τ at different atmospheric conditions

Stability conditions	Height (m)	Angle of Attack		τ (Nm^{-2})	H (Wm^{-2})
		Range	Mean values		
Unstable	18	$\pm 6^\circ$	$+0.8^\circ \pm 3.32^\circ$	0.22 ± 0.13	145 ± 88
	30	$\pm 6^\circ$	$+1^\circ \pm 2.61^\circ$	0.25 ± 0.16	144 ± 92
Neutral	18	$\pm 6^\circ$	$+0.58^\circ \pm 2.27^\circ$	0.14 ± 0.11	5.85 ± 24
	30	$\pm 6^\circ$	$+1.4^\circ \pm 3.23^\circ$	0.14 ± 0.12	-5.0 ± 12
Stable	18	$\pm 6^\circ$	$-0.7^\circ \pm 3.15^\circ$	0.038 ± 0.04	-12 ± 19
	30	$\pm 6^\circ$	$-0.9^\circ \pm 2.26^\circ$	0.04 ± 0.05	-13 ± 20

the heterogeneous topography and wind direction variability on the surface fluxes. SPF introduces an instrument's offset value in w for different wind dominant sectors. The offset values showed the over- and underestimation of surface fluxes by the sensor at the station. As a result of SPF, the instrument's offset values are reduced compared to GPF values, which indicates a minimization of planar fit error in the computation. DR computed larger momentum flux values compared to PF methods. For sensible heat flux, 12–13% variation has been seen in day and night fluxes between the GPF and SPF computed values, while Momentum flux varied in the range of 16–18% between the GPF and SPF computed values during day hours. The difference can be attributed to different characteristics of slope, flow direction, and moderate wind speed, which are not considered into account in planar-fit. There is a large difference in the vertical wind value between the GPF and SPF technique, which indicates that at the station wind direction variability has an important role in surface flux estimation. SPF was able to reduce the impact of wind direction variability and heterogeneity of the terrain on the surface fluxes. So it can be concluded that the SPF is very useful over a complex site like NESAC, Umiam, where the wind direction changed drastically at the regular intervals.

The fluctuation of standard deviations of u and w wind components normalized by u_* (σ_u/u_* and σ_w/u_*) as a function of atmospheric stability (z/L) follows a power-law relation during stable and unstable conditions, with a small variation in fitted coefficients. The fitted coefficients estimated from the above variations are in good agreement with those estimated over both flat and mountainous site by Foken et al. (1991) and Foken and Wichura (1996). This exercise further reinforces that the statistics and parameterization of turbulence characteristics in the ABL over mountainous station are like those over a plain homogeneous surface, at least for the low to moderate winds observed at the station.

Acknowledgements This investigation has been carried out as part of the IGBP-NOBLE project. We thank the Director, Director SPL, and Project Director, ISRO-IGBP for their valuable support.

References

Avissar R, Chen F (1993) Development and analysis of prognostic equations for mesoscale kinetic energy and mesoscale (sub-grid scale) fluxes for large-scale atmospheric models. *J Atmos Sci*. [https://doi.org/10.1175/1520-0469\(1993\)050%3C3751:DAAOPE%3E2.0.CO;2](https://doi.org/10.1175/1520-0469(1993)050%3C3751:DAAOPE%3E2.0.CO;2)

- Baldocchi DD, Harley P (1995) Scaling carbon dioxide and water vapor exchange from leaf to canopy in a deciduous forest: model testing and application. *Plant Cell Environ* 18(10):1146–115. <https://doi.org/10.1111/j.1365-3040.1995.tb00625.x>
- Berger BW, Davis KJ, Yi C, Bakwin PS, Zhao C (2001) Long-term carbon dioxide fluxes from a very tall tower in a northern forest: Part I. Flux measurement methodology. *J Atmos Oceanic Technol* 18:529–542
- Bianco L, Djalalova IV, King CW, Wilczak JM (2011) Diurnal evolution and annual variability of boundary layer height and its correlation with other meteorological variables in California's Central Valley. *Bound-Layer Meteorol* 140:491–511. <https://doi.org/10.1007/s10546-011-9622-4>
- Black TA, den Hartog G, Neumann HH, Blanken PD, Yang PC, Russell C, Nesic Z, Lee X, Chen SG, Staebler R, Novak MD (1996) Annual cycles of water vapor and carbon dioxide fluxes in and above a boreal aspen forest. *Global Change Biol.* <https://doi.org/10.1111/j.1365-2486.1996.tb00074.x>
- CSAT3 (2014) Instruction manual: CSAT3 three dimensional sonic anemometer. Campbell Scientific. Inc
- Finnigan JJ (1999) A comment on the paper by Lee (1998): on micrometeorological observations of surface-air exchange over tall vegetation. *Agri For Meteorol* 97:55–64
- Finnigan JJ, Clement R, Malhi Y, Leuning R, Cleugh HA (2003) A re-evaluation of long-term flux measurement techniques. Part I. Averaging and coordinate rotation. *Bound-Layer Meteorol* 107:1–48
- Foken T, Wichura B (1996) Tools for quality assessment of surface-based flux measurements. *Agri For Meteorol* 78(1–2):83–105
- Foken T, Skeib G, Richter SH (1991) Dependence of the integral turbulence characteristics on the stability of stratification and their use for Doppler-Sodar measurements. *Z Meteorol* 41:311–315
- Foken T, Gockede M, Mauder M, Mahrt L, Amiro BD, Munger JW (2004) Post-field data quality control. In: Lee X, Massman WJ, Law BE (eds) *Handbook of micrometeorology. A guide for surface flux measurements*. Dordrecht, Kluwer, pp 181–208
- Fuentes JD, Gillespie TJ, den Hartog G, Neumann HH (1992) Ozone deposition onto a deciduous forest during dry and wet conditions. *Agri For Meteorol* 62:1–18. [https://doi.org/10.1016/0168-1923\(92\)90002-L](https://doi.org/10.1016/0168-1923(92)90002-L)
- Gash JHC, Dolman AJ (2003) Sonic anemometer (co)sine response, and flux measurement. I. The potential for (co)sine error to affect sonic anemometer-based flux measurements. *Agri For Meteorol* 119:195–207
- Geissbuhler P, Siegwolf R, Eugster W (2000) Eddy covariance measurements on mountain slopes: the advantage of surface-normal sensor orientation over a vertical set-up. *Bound-Layer Meteorol* 96:371–392
- Goulden ML, Munger JW, Fan SM, Daube BC, Wofsy SC (1996) Exchange of carbon dioxide by a deciduous forest: response to interannual climate variability. *Science* 271:1576–1578. <https://doi.org/10.1126/science.271.5255.1576>
- Grace J, Lloyd J, McIntyre J, Miranda AC, Meir P, Miranda HS, Nobre C, Moncrieff J, Mashedier J, Malhi Y, Wright I, Gash J (1995) Carbon dioxide uptake by an undisturbed tropical rain forest in southwest Amazonia, 1992–1993. *Science* 270:778–780. <https://doi.org/10.1126/science.270.5237.778>
- Guenther A, Baugh W, Davis K, Hampton G, Harley P, Klinger L, Vierling L, Zimmerman P, Allwine E, Dilts S, Lamb B, Westbeg H, Baldocchi D, Geron C, Pierce T (1996) Isoprene fluxes measured by enclosure, relaxed eddy accumulation, surface layer gradient, mixed layer gradient and mixed layer mass balance techniques. *J Geophys Res* 101(D13):18555–18567. <https://doi.org/10.1029/96JD00697>
- Hollinger DY, Kelliher FM, Byers JN, Hunt JE, McSeveny TM, Weir PL (1994) Carbon dioxide exchange between an undisturbed old-growth temperate forest and the atmosphere. *Ecology* 75(1):134–150. <https://doi.org/10.2307/1939390>
- Kral ST, Sjöblom A, Nygård T (2014) Observations of summer turbulent surface fluxes in a High Arctic fjord. *Q J R Meteorol Soc* 140:666–675. <https://doi.org/10.1002/qj.2167>
- Lee X (1998) On micrometeorological observations of surface-air exchange over tall vegetation. *Agri For Meteorol* 91:39–49
- Lee X, Massman W, Law BE (2004) *Handbook of micrometeorology. A guide for flux measurement and analysis*. Kluwer Academic Press, Dordrecht
- Li M, Babel W, Tanaka K, Foken T (2013) Note on the application of planar-fit rotation for non-Omnidirectional sonic anemometers. *Atmos Meas Tech* 6:221–229. <https://doi.org/10.5194/amt-6-221-2013>
- Liang J, Zhang L, Wang Y, Cao X, Zhang Q, Wang H, Zhang B (2014) Turbulence regimes and the validity of similarity theory in the stable boundary layer over complex terrain of the Loess Plateau. *China J Geophys Res Atmos* 119:6009–6021. <https://doi.org/10.1002/2014JD021510>
- Lindberg SE, Hanson PJ, Meyers TP, Kim KH (1998) Air/surface exchange of mercury vapor over forests, the need for a reassessment of continental biogenic emissions. *Atmos Environ Elsevier* 32(5):895–908. [https://doi.org/10.1016/S1352-2310\(97\)00173-8](https://doi.org/10.1016/S1352-2310(97)00173-8)
- Mahrt L, Sun J (1995) Dependence of surface exchange coefficients on the averaging scale and grid size. *Quart J R Meteorol Soc* 121
- Mammarella I, Kolari P, Rinne J, Keromen P, Pumpanen J, Vesala T (2007) Determining the contribution of vertical advection to the net ecosystem exchange at Hyytiälä Forest. *Finland Tellus* 59B:900–909. <https://doi.org/10.1111/j.1600-0889.2007.00306.x>
- McBean GA (1974) The turbulent transfer mechanisms: a time domain analysis. *Q J Roy Meteorol Soc* 100:53–66
- McMillen RT (1988) An eddy correlation technique with extended applicability to non-simple terrain. *Bound-Layer Meteorol* 43(3):231–245. <https://doi.org/10.1007/BF00128405>
- Monin AS, Obukhov AM (1954) Basic laws of turbulent mixing in the surface layer of the atmosphere. *Tr. Akad Nauk SSSR Geophys Inst* 24:163–187
- Moraes OLL, Acevedo OC, Degrazia GA, Anfossi D, da Silva R, Anabor V (2005) Surface layer turbulence parameters over a complex terrain. *Atmos Environ* 39:3103–3112
- Motha RP, Verma SB, Rosenberg NJ (1980) Turbulence spectra above a vegetated surface under conditions of sensible heat advection. *J Appl Meteorol* 18:317–323
- Oldroyd HJ, Pardyjak ER, Huwald H, Parlange MB (2016) Adapting tilt corrections and the governing flow equations for steep, fully three-dimensional, mountainous terrain. *Bound-Layer Meteorol* 159:539–565. <https://doi.org/10.1007/s10546-015-0066-0>
- Ono K, Mano M, Miyata A, Inoue Y (2008) Applicability of the planar-fit technique in estimating surface-fluxes over flat terrain using eddy covariance. *J Agri Meteorol* 64:121–130. <https://doi.org/10.2480/agrmet.64.3.5>
- Paw UKT, Baldocchi DD, Meyers TP, Wilson K (2000) Correction of Eddy-covariance measurements incorporating both advective effects and density fluxes. *Bound-layer Meteorol* 97:487–511
- Rebmann C, Kolle O, Heinesch B, Queck R, Ibrom A, Aubinet M (2012) Data acquisition and flux calculations. Eddy covariance: a practical guide to measurement and data analysis. Springer Atmos Sci 59–83. ISBN 978-94-007-2351-1
- Rotach MW, Zardi D (2007) On the boundary-layer structure over highly complex terrain: key findings from MAP. *Q J R Meteorol Soc* 133:937–948. <https://doi.org/10.1002/qj.71>
- Shimizu T (2015) Effect of coordinate rotation systems on calculated fluxes over a forest in complex terrain: a comprehensive comparison. *Bound-Layer Meteorol.* <https://doi.org/10.1007/s10546-015-0027-7>

- Siebicke L, Hunner M, Foken T (2012) Aspects of CO₂ advection measurements. *Theor Appl Climatol* 109:109–131. <https://doi.org/10.1007/s00704-011-0552-3>
- Solanki R, Singh N, Kiran Kumar NVP, Rajeev K, Dhaka SK (2016) Time variability of surface-layer characteristics over a mountain ridge in the central himalayas during the spring season. *Springer Bound-Layer Meteorol* 158:453–471. <https://doi.org/10.1007/s10546-015-0098-5>
- Stiperski I, Rotach MW (2016) On the measurement of turbulence over complex mountainous terrain. *Bound-Layer Meteorol* 159:97–121. <https://doi.org/10.1007/s10546-015-0103-z>
- Stull RB (1988) An introduction to boundary layer meteorology. Kluwer Academic Publishers, Dordrecht
- Turnipseed AA, Anderson DE, Blanken PD, Baugh WM, Monson RK (2003) Airflows and turbulent flux measurements in mountainous terrain Part 1. Canopy and local effects. *Agric For Meteorol* 119:1–21. [https://doi.org/10.1016/S0168-1923\(03\)00136-9](https://doi.org/10.1016/S0168-1923(03)00136-9)
- van der Molen MK, Gash JHC, Elbers JA (2004) Sonic anemometer (co)sine response and flux measurement: II. The effect of introducing an angle of attack dependent calibration. *Agric For Meteorol* 122:95–109
- Verma SB, Baldocchi DD, Anderson DE, Matt DR, Clement RJ (1986) Eddy fluxes of CO₂, water vapor, and sensible heat over a deciduous forest. *Bound-Layer Meteorol* 36(1–2):71–91. <https://doi.org/10.1007/BF00117459>
- Vickers D, Mahrt L (2006) A solution for flux contamination by mesoscale motions with very weak turbulence. *Bound-Layer Meteorol* 11:431–447
- Wilczak JM, Oncley SP, Stage S (2001) Sonic anemometer tilts correction algorithms. *Bound-Layer Meteorol* 99:127–150
- Yuan R, Kang M, Park S, Hong J, Lee D, Kim J (2007) The effect of coordinate rotation on the eddy covariance flux estimation in a hilly ko-flux forest catchment. *Korean J Agri For Meteorol* 9(2):100–108
- Yuan R, Kang M, Park S (2011) Expansion of the planar-fit method to estimate flux over complex Terrain. *Meteorol Atmos Phys* 110:123–133. <https://doi.org/10.1007/s00703-010-0113-9>

Publisher's Note Springer Nature remains neutral with regard to jurisdictional claims in published maps and institutional affiliations.